Structure and Morphology Evolution of Hematite (α-Fe_2O_3) Nanoparticles in Forced Hydrolysis of Ferric Chloride

Wei Wang,*,† Jane Y. Howe,‡ and Baohua Gu†

Environmental Sciences Division, Oak Ridge National Laboratory, P.O. Box 2008, Oak Ridge, Tennessee 37831, and Materials Sciences and Technology Division, Oak Ridge National Laboratory, P.O. Box 2008, Oak Ridge, Tennessee 37831

Received: January 23, 2008; Revised Manuscript Received: March 31, 2008

Hematite (α-Fe_2O_3) nanoparticles were prepared by forced hydrolysis of ferric chloride under acidic pH conditions. Without introduction of any additives, hematite nanoparticles with varying sizes and morphologies were obtained by controlling the nucleation rate, Fe^{3+} concentration, and aging time. Synthesized primary nanocrystals show such morphologies as cubic, spherical, sheetlike, and hexagonal structures and unusual disklike and tetrahedral aggregates. In addition to previous findings that phase transformation usually occurs from akaganeite (β-FeOOH) to hematite during forced hydrolysis, direct transformation of amorphous iron oxides to crystalline hematite at an early stage of hydrolysis were also observed and confirmed by X-ray diffraction and Raman spectroscopic analysis.

Introduction

Synthetic iron oxides have been widely used in commercial and industrial applications such as pigments, catalysts, adsorbents, magnetic materials, and sensors.[1,2] Since Matijević and co-workers reported the preparation of hematite (α-Fe_2O_3) colloidal particles by forced hydrolysis or hydrothermal reactions in dilute Fe(III) salt solution,[3,4] extensive studies have been carried out in investigating the formation mechanisms and morphological controls for the synthesis of α-Fe_2O_3 nanoparticles. It has been known that the hydrolysis of Fe^{3+} and the formation of iron oxide nanocrystals strongly depend on, among other factors, solution pH, reaction temperature, aging time, solvents, and the type of Fe(III) salt and its concentration.[5–16] In forced hydrolysis of Fe(III) salts, morphologies of α-Fe_2O_3 nanoparticles are strongly influenced by organic/inorganic additives, such as inorganic salts[10,17–22] or organic compounds.[23–29] For examples, single-crystalline α-Fe_2O_3 nanotubes could be formed in existence of $NH_4H_2PO_4$,[22] while nanorods of α-Fe_2O_3 with a high aspect ratio could be obtained with assistance of cationic surfactant, cetyltrimethylammonium bromide (CTAB).[29] Depending on the addition of various organic or inorganic additives, the formation processes of hematite particles are usually thought to contain a phase transfer process either from akaganeite (β-FeOOH) to α-Fe_2O_3[4,9,11,22,23,30] by using $FeCl_3$, or from goethite (α-FeOOH) to α-Fe_2O_3 by using $Fe(NO_3)_3$.[7] However, detailed formation mechanism of α-Fe_2O_3 nanocrystals, especially in early stage of the hydrolysis reaction, is still not fully understood. In this work, we investigated the effect of nucleation rate, reactant concentration, and aging time on the formation and morphological properties of synthesized hematite by forced hydrolysis under acidic pH conditions. Without introducing any additives, we report that hematite nanoparticles with varying sizes and morphologies can be synthesized via a direct phase transformation from amorphous iron oxides to α-Fe_2O_3.

Experimental Section

Anhydrous ferric chloride ($\geq$98%) and hydrochloric acid (GR) were purchased form EM Sciences and used for the preparation of the $FeCl_3$ and HCl stock solutions. Hydrolysis experiments were performed at 100 °C ($\pm$1 °C) under two different nucleation processes: (1) a slow nucleation, in which stock solutions were mixed with deionized water in a glass bottle at room temperature, and the reaction mixture was heated to 100 °C by 8 °C/min in a water bath, and (2) a fast nucleation, in which the stock solution was quickly poured into boiling deionized water under vigorous stirring, and the reaction mixture was kept at 100 °C without further mixing.

The size and morphology of synthesized nanoparticles were evaluated by both transmission and scanning electron microscopic analyses. A Hitachi HF-2000 transmission electron microscope (TEM) under an acceleration voltage of 200 kV and a Hitachi S-4700 scanning electron microscope (SEM) operated at 15 kV were used for direct imaging of synthesized colloidal nanoparticles. A drop of the colloid suspension was placed and dried on a lacey carbon film supported by a 200-mesh Cu grid for TEM observations. For SEM analysis, a drop of colloid suspension was placed on a piece of copper foil and coated with iridium before analysis. The crystalline structure of synthesized nanoparticles was identified by Raman spectroscopy using a Renishaw Raman spectrometer equipped with a Leica microscope and a 785-nm diode laser. The spectral resolution was $\sim$2 cm^{-1}. A drop of the colloid suspension was placed on a quartz slide and allowed to dry before Raman scattering measurements. The laser power was set at $\sim$20 mW at the exit of the microscope objective. The crystalline structure was also examined by X-ray diffraction (XRD) analysis with a Scintag XRD 2000 powder diffractometer.

* To whom correspondence should be addressed. E-mail: wangw@ornl.gov. Fax: 865-576-3989.
† Environmental Sciences Division.
‡ Materials Science and Technology Divisions.

10.1021/jp800683j CCC: $40.75
Published on Web 06/03/2008

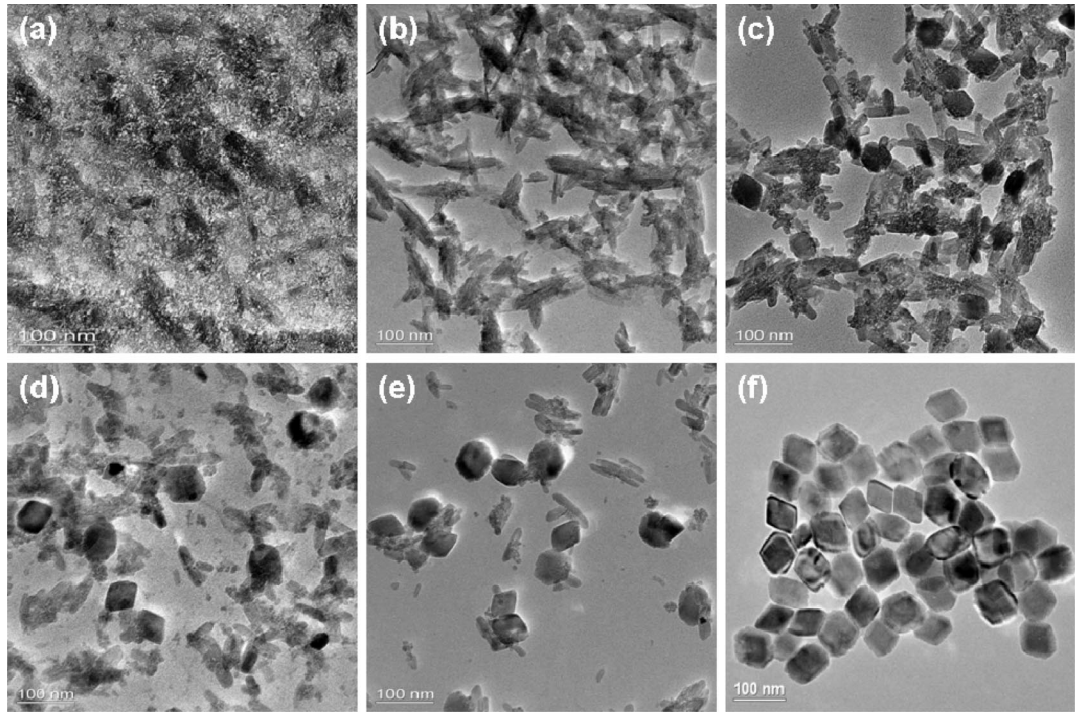

Figure 1. TEM images of as-synthesized hematite nanocrystals by a slow nucleation process at various aging times of (a) 15 min, (b) 1 h, (c) 4 h, (d) 8 h, (e) 16 h, and (f) 48 h at 100 °C. The initial reactant concentrations were 1×10^{-2} M $FeCl_3$ and 2×10^{-3} M HCl.

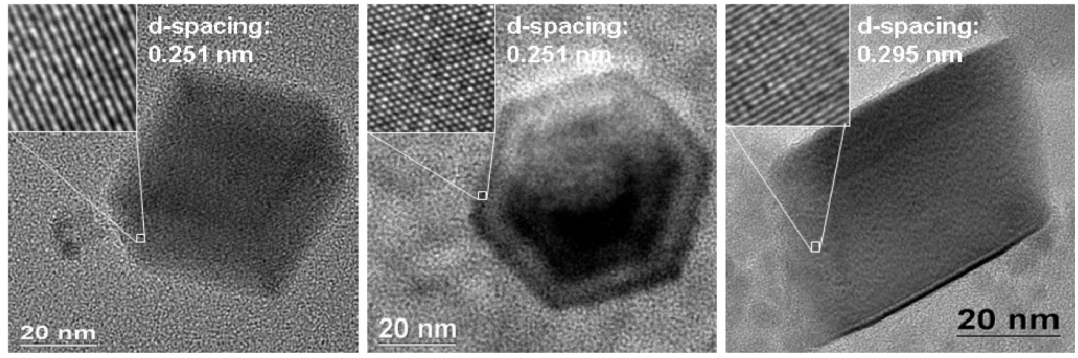

Figure 2. High-resolution TEM images of iron oxide nanocrystals of different morphologies: (a) cubic hematite, $d = 0.251$ nm, 110 crystal face, (b) hexagonal hematite, $d = 0.251$ nm, 110 crystal face, and (c) sheetlike maghemite, $d = 0.295$ nm, 220 crystal face.

Results and Discussion

Effect of Aging Time on Particle Growth and Transformation. The effect of aging time on the size and morphology of α-Fe_2O_3 nanocrystals was first examined under slow nucleation conditions at initial reactant concentrations of 1×10^{-2} M $FeCl_3$ and 2×10^{-3} M HCl at 100 °C (Figure 1). Results indicated that primary particles first formed as aggregates with irregular shapes at an early stage of the hydrolysis (Figure 1a, aged for 15 min). With an increase of aging time, irregularly shaped particles transformed into bar-shaped nanoparticles (aged for 1−2 h), followed by the appearance of quasi-cubic-shaped nanoparticles (aged for 4 h). At aging time of 8−16 h, a large fraction of these bar-shaped nanoparticles transformed into cubic shaped particles (parts d and e of Figure 1d and e), and ultimately all bar-shaped particles became large cubic α-Fe_2O_3 nanoparticles (~80−90 nm in size) at an aging time of 48 h (Figure 1f). A close examination of the morphology of these particles also revealed the presence of a few sheet or hexagonal shaped nanocrystals. High-resolution TEM images revealed that these cubic and hexagonally shaped particles have a d spacing of 0.251 nm (Figure 2), corresponding to 111 plane of hematite structure, as expected, and confirmed by RDX. However, the sheetlike nanocrystals exhibit a d spacing of 0.295 nm, corresponding to the 220 plane of the maghemite (γ-Fe_2O_3) structure. This is an interesting observation because sheetlike maghemite impurities were not reported in the synthesis of hematite by forced hydrolysis. Additionally, alternative bright and dark fields (or stripes) were observed for hexagonally shaped hematite nanocrystals (Figure 2b) as well for some cubic-shaped nanocrystals (Figure 1f and 5c) in TEM images. This phenomenon was previously attributed to the presence of multilayer cage structures of hematite nanoparticles by X. Wang et al.[27] However, we believe that the phenomenon originates from thickness fringes in electron microscopy as evidenced by the high-resolution TEM image (Figure 3), showing three bright and dark fields or stripes from a single hematite nanocrystal.

Hematite belongs to the D^6_{3d} crystal group. Seven phonon lines (two A_{1g} modes, 225 and 498 cm^{-1}, and five E_g modes,

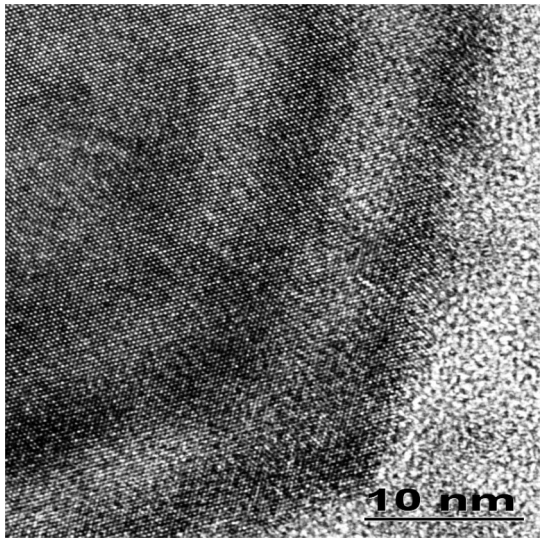

Figure 3. High-resolution TEM image of the edge of a hexagonal shaped hematite nanocrystal showing thickness fringes as three alternative bright and dark fields or stripes.

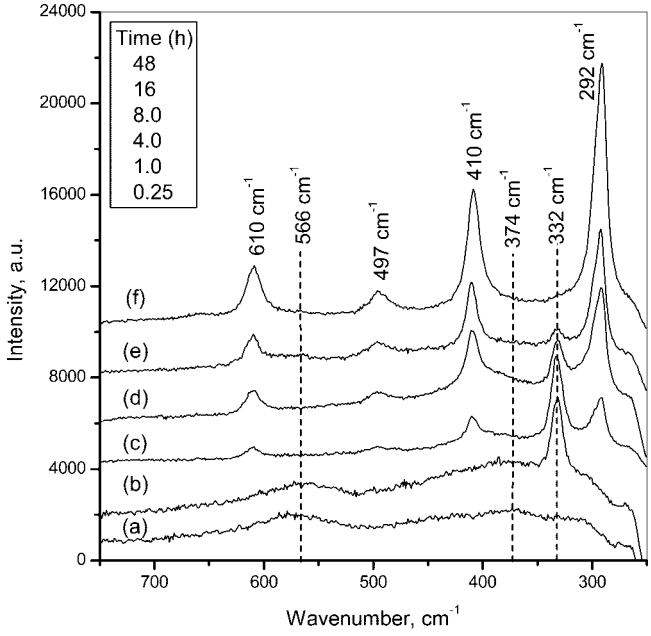

Figure 4. Raman spectroscopic analysis of particle structural evolution from amorphous iron oxide to hematite at different stages of the hydrolysis under a slow nucleation process.

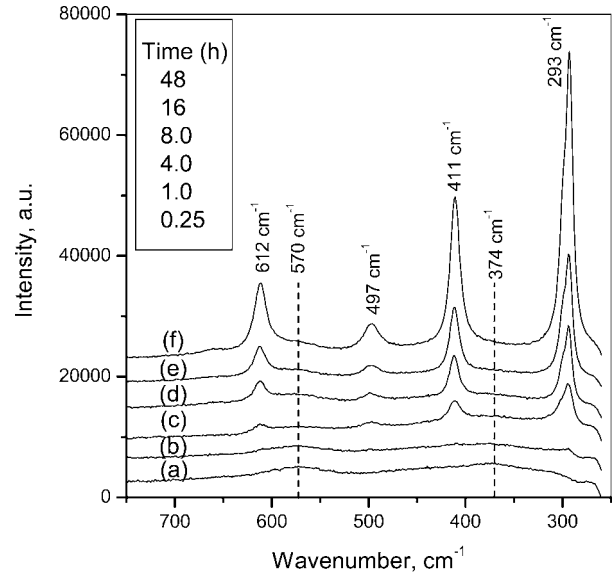

Figure 6. Raman spectra of as-synthesized amorphous iron oxide and hematite nanocrystals by the fast nucleation process at different stages of the hydrolysis.

247, 293, 299, 412, and 613 cm^{-1}) are expected in its Raman spectrum.[31–33] We monitored the particle structural evolution using Raman spectroscopy (Figure 4). At an early stage of the hydrolysis (<0.5 h), no clear vibrational bands could be identified except weak broad bands at around 566 and 374 cm^{-1} due to amorphous iron oxides (Figure 4a). With an increase in aging time (1 h), a band at 332 cm^{-1} appeared (Figure 4b) and might be attributed to β-FeOOH structures, corresponding to the formation of bar-shaped nanoparticles (Figure 1b). With further increasing aging time in hydrolysis, spectra show the evolution of α-Fe_2O_3 with characteristic bands at 610 (E_g), 497 (A_{1g}), 410 (E_g), and 292 cm^{-1} (E_g) (Figure 4c), which also coincide with the appearance of cubic shaped hematite nanoparticles shown in parts c−f of Figure 1. As expected, band intensities of α-Fe_2O_3 increased, whereas that of β-FeOOH decreased with increase of hydrolysis time (parts c−e of Figure 4). At 48 h, the band at 332 cm^{-1} completely disappeared, and only pure-phase α-Fe_2O_3 was observed (Figure 4f). Therefore, Raman spectroscopic analysis provided direct evidence of structural transformation of bar-shaped β-FeOOH and the evolution of cubic dominant α-Fe_2O_3 nanoparticles during the forced hydrolysis. These observations are in good agreement with those reported in the literature.[9,11,15,26] We note that maghemite

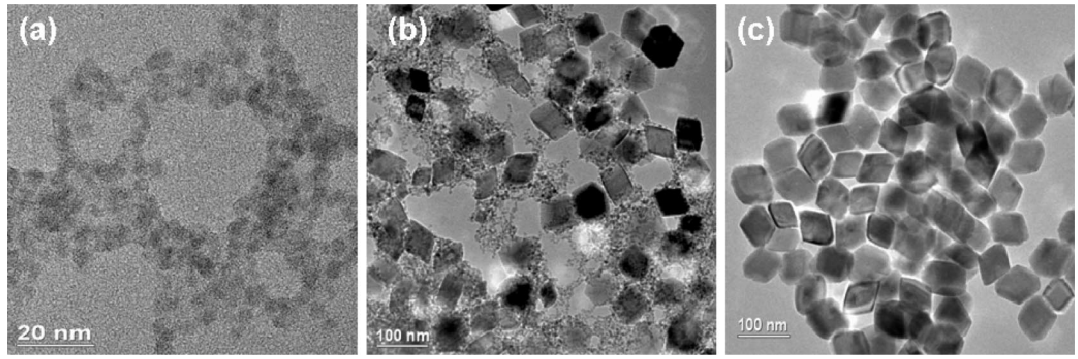

Figure 5. TEM images of as-synthesized hematite nanocrystals by the fast nucleation process with an aging time of (a) 15 min, (b) 16 h, and (c) 48 h. The initial reactant concentrations were 1×10^{-2} M $FeCl_3$ and 2×10^{-3} M HCl at 100 °C.

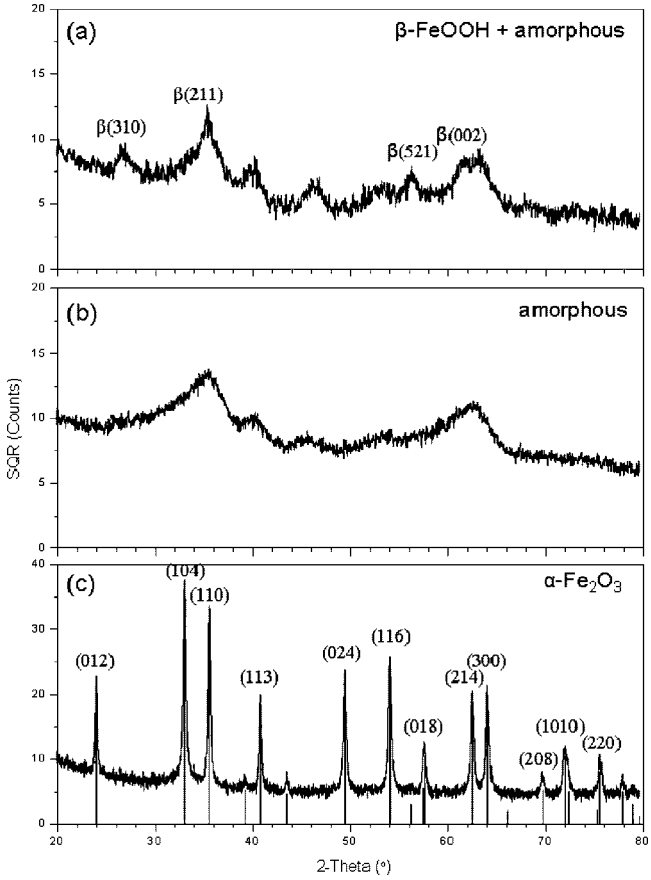

Figure 7. XRD patterns of as-synthesized iron oxide nanoparticles formed in a slow nucleation process at an aging time of 30 min (a) and in a fast nucleation process at aging times of 30 min (b) and 48 h (c). The initial reactant concentrations were 1×10^{-2} M $FeCl_3$ and 2×10^{-3} M HCl.

structures were neither identified in Raman nor XRD because of its extremely low fraction in α-Fe_2O_3 as impurities.

Effect of Nucleation Rate on Particle Formation. The rate of nucleation during forced hydrolysis appeared to have a significant influence in particle transformation. Previous mechanistic studies indicate that α-Fe_2O_3 nanocrystals are formed by the phase transformation from β-FeOOH or α-FeOOH during forced hydrolysis. [4,7,9,11,22,23,30] Here we report that a direct phase transformation from amorphous iron oxides to hematite nanocrystals through a rapid nucleation process. Under the same initial conditions (with respect to reactant concentrations and temperature), the rapid nucleation process first produced small spherical iron oxide nanoparticles (Figure 5a), instead of irregular or bar-shaped nanoparticles as observed in the slow nucleation process (parst a and b of Figure 1). Within the early stage of the hydrolysis (<2 h), Raman spectroscopic analysis showed no characteristic scattering bands of either β-FeOOH or α-Fe_2O_3, suggesting the formation of amorphous ferric oxides initially (parts a and b of Figure 6). With increasing aging time, cubic shaped α-Fe_2O_3 nanocrystals formed whereas primary spherical nanoparticles gradually disappeared (parts b and c of Figure 5). Ultimately (48 h), all primary particles transformed to cubic-shaped α-Fe_2O_3 nanoparticles with a size range from ~80 to 90 nm (Figure 5c), which are essentially the same as those formed in the slow nucleation process (Figure 1f). Again, no Raman scattering bands of β-FeOOH were observed, but the phase transformation coincided with increased intensities of Raman scattering bands at 612, 497, 411, and 293 cm^{-1} (parts c−f of Figure 6), thereby providing additional evidence of the structural transformation from amorphous Fe_2O_3 to hematite nanocrystals. XRD analyses (Figure 7) also slowed only amorphous structures at an early stage of hydrolysis by the fast nucleation process. We can thus reasonably conclude that the rate of nucleation leads to different mechanisms of phase transformation and the growth of Fe_2O_3 particles in the forced hydrolysis of Fe^{3+}.

Effect of Ferric Ion Concentration on Particle Growth. The particle morphology evolution by the fast nucleation process was also studied under varying Fe^{3+} concentrations while holding the HCl concentration constant at 2×10^{-3} M at 100 °C. Different sizes and morphologies of hematite nanocrystals were obtained at an aging time of 16 h (Figure 8). At a low Fe^{3+} concentration (1.25×10^{-3} M), only small spherical α-Fe_2O_3 particles (~5−10 nm) were obtained. With an increase in the Fe^{3+} concentration (at 2.5, 5, and 7.5 mM), larger particles in the size range of ~30−50, ~40−60, and ~50−70 nm were formed over small spherical primary particles. These results suggest the importance in controlling the initial Fe^{3+} concentration so that different sized and shaped iron oxide nanocrystals can be obtained.

Furthermore, primary cubic-shaped α-Fe_2O_3 particles were found to self-assemble into disklike aggregates when the reaction media slowly evaporated to three-fourth of its original volume in 48 h, and the size of the disks depended on the initial Fe^{3+} concentration (Figure 9). If the reaction media was evaporated to half of its original volume in a period of 16 h, primary particles self-assmbled to form large tetrahedral aggregate structures (~1−3 μm in dimension, Figure 10). We note that some nanoparticles moved to and concentrated at the air/water interface during solvent evaporation, which may have resulted from an increased hydrophobicity by losing surface hydroxyl groups on α-Fe_2O_3 and thus promoted the formation of these large particle aggregates. These disklike and tetrahedral particles aggregate were also found to be stable in suspension and could not be broken up into primary nanocrystals by sonification. Such disklike particle aggregates have been observed previously only in hydrothermal hydrolysis of ferric chelates at high temperatures (≥180 °C)[5,8,34] or in the presence of additives such as polyvinyl alcohol.[25] To our knowledge, this is the first report that tetrahedral and disk-shaped hematite nanoparticles or aggregates are formed by forced hydrolysis at a relatively low temperature (100 °C) without introducing any chelates or additives. These observations again demonstrate the dependence of the particle size and morphology on nucleation rates and the Fe^{3+} concentration during forced hydrolysis of Fe^{3+}.

Conclusions

Despite extensive studies of the forced hydrolysis of $FeCl_3$ under acidic pH conditions, this study demonstrates that, without introducing any organic or inorganic additives, the size and morphology of synthesized hematite nanoparticles could be controlled by varying the Fe^{3+} concentration, nucleation rate, and aging time. Raman spectroscopic analysis revealed two different structural evolution routes during the growth of hematite nanoparticles. At an early stage of the hydrolysis reaction, a slow nucleation process resulted in the formation of irregularly shaped amorphous structure and then bar-shaped β-FeOOH primary particles, while a fast nucleation process produced spherical primary particles with amorphous structures. With increasing aging time, however, both bar-shaped and spherical primary particles eventually all transformed into cubic shaped hematite nanocrystals. In

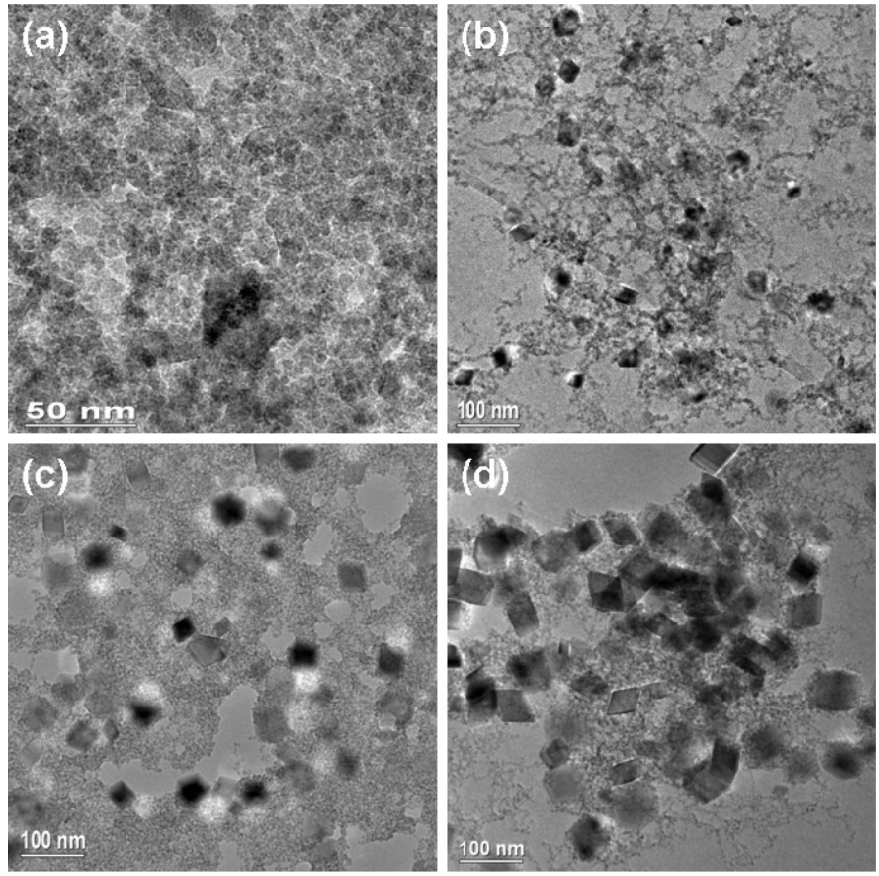

Figure 8. TEM images of as-synthesized hematite nanocrystals by the fast nucleation process at a fixed HCl concentration of 2 mM but varying concentrations of $FeCl_3$ at (a) 1.25, (b) 2.5, (c) 5, and (d) 7.5 mM. Samples were aged for 16 h at 100 °C.

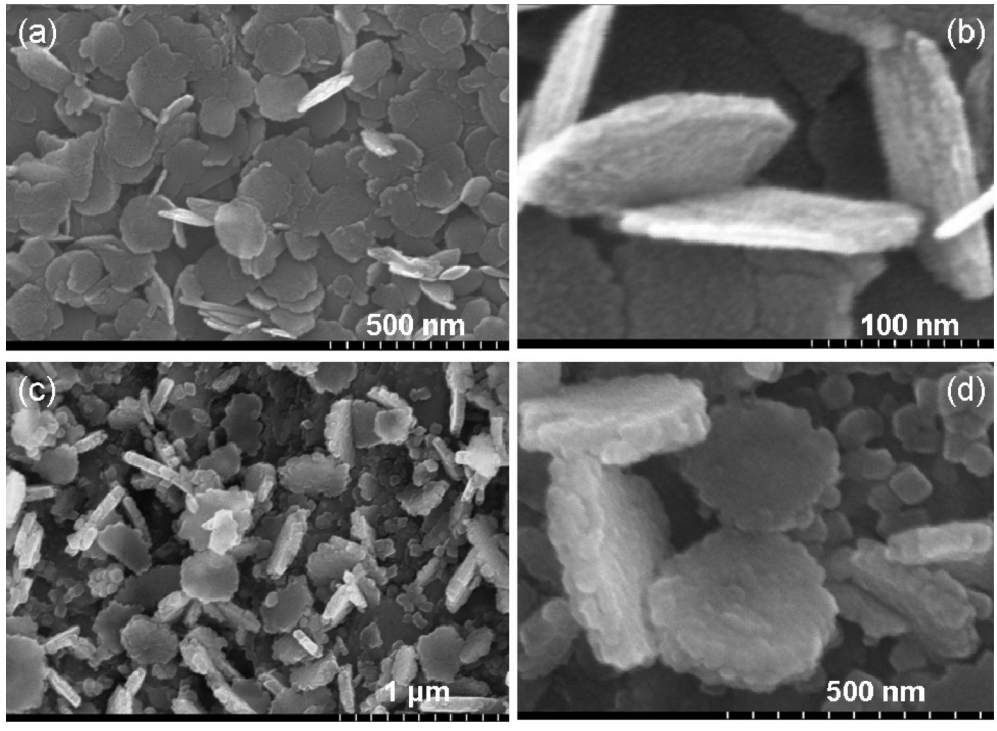

Figure 9. SEM images of disklike hematite particle aggregates formed by the fast nucleation process at 100 °C with an aging time of 48 h. Solvent was evaporated to about three-fourths of its original volume during the reaction period. The initial reactant concentrations were 2×10^{-3} M (a,b) and 1×10^{-2} M (c,d) $FeCl_3$ in 2×10^{-3} M HCl solution.

contrast to previous findings that phase transformation usually occurs from β-FeOOH to hematite, direct transformation of amorphous iron oxides to crystalline hematite was observed during the fast nucleation process. For the first time, we found that primary hematite nanoparticles readily self-assemble into large aggregates of unusual morphologies such as disklike

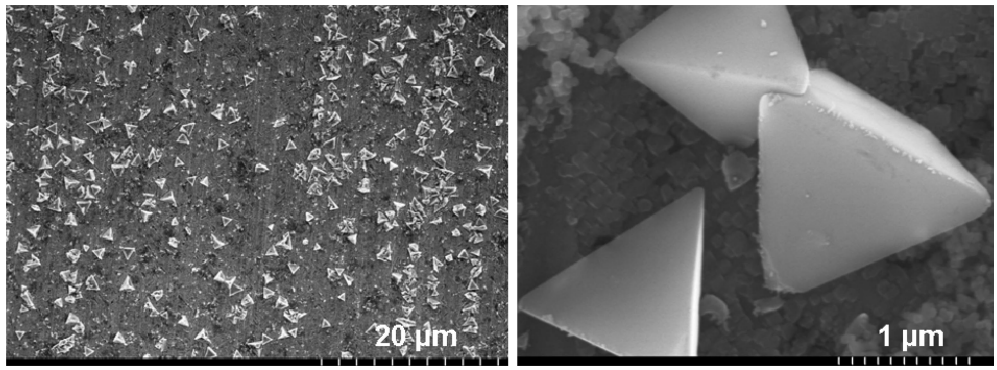

Figure 10. SEM images of tetrahedral-like hematite particle aggregates formed by the fast nucleation process at 100 °C with an aging time of 16 h. The solvent was evaporated to half of its original volume during the reaction period, and initial reactant concentrations were 1×10^{-2} M $FeCl_3$ and 2×10^{-3} M HCl.

and tetrahedral structures by evaporating solvent during the thermal hydrolysis reaction.

Acknowledgment. We thank Dr. R. A. Meisner for performing the XRD measurements. This research was sponsored by the Laboratory Directed Research and Development (LDRD) Program of Oak Ridge National Laboratory (ORNL) which is managed by UT−Battelle, LLC, for the U.S. Department of Energy under Contract No. DE-AC05-00OR22725.

References and Notes

(1) Matijević, E. *Chem. Mater.* **1993**, *5*, 412.
(2) Flynn, C. M., Jr *Chem. Rev.* **1984**, *84*, 31.
(3) Matijević, E. *J. Colloid Interface Sci.* **1977**, *58*, 374.
(4) Matijević, E.; Scheiner, P. *J. Colloid Interface Sci.* **1978**, *63*, 509.
(5) Ozaki, M.; Ookoshi, N.; Matijević, E. *J. Colloid Interface Sci.* **1990**, *137*, 546.
(6) Bailey, J. K.; Brinker, C. J.; Mecartney, M. L. J. *Collloid Interafce Sci.* **1993**, *157*, 1.
(7) Gotić, M.; Popović, S.; Ljubešić, N.; Musić, S. *J. Mater. Sci.* **1994**, *29*, 2474.
(8) Sugimoto, T.; Muramatsu, A.; Sakata, K.; Shindo, D. J. *Colloid Interface Sci.* **1993**, *158*, 420.
(9) Sugimoto, T.; Muramatsu, A. *J. Colloid Interface.* **1996**, *184*, 626.
(10) Sugimoto, T.; Wang, Y.; Itoh, H.; Muramatsu, A. *Colloids Surf. A* **1998**, *134*, 265.
(11) Kan, S.; Yu, S.; Peng, X.; Zhang, X.; Li, D.; Xiao, L.; Zou, G.; Li, T. *J. Colloid Interface Sci.* **1996**, *178*, 673.
(12) Kan, S.; Zhang, X.; Yu, S.; Li, D.; Xiao, L.; Zou, G.; Li, T.; Dong, W.; Lu, Y. *J. Colloid Interface Sci.* **1997**, *191*, 503.
(13) Kandori, K.; Sakai, J.; Ishikawa, T. *Phys. Chem. Chem. Phys.* **2000**, *2*, 3293.
(14) Katsuki, H.; Komarneni, S. *J. Am. Ceram. Soc.* **2001**, *84*, 2313.
(15) Musić, S.; Krehula, S.; Popović, S. *Mater. Lett.* **2004**, *58*, 2640.
(16) Liang, X.; Wang, X.; Zhuang, J.; Chen, Y.; Wang, D.; Li, Y. *Adv. Funct. Mater.* **2006**, *16*, 1805.
(17) Ozaki, M.; Kratohvil, S.; Matijević, E. *J. Colloid Interface Sci.* **1984**, *102*, 146.
(18) Reeves, N. J.; Mann, S. *J. Chem. Soc. Faraday Trans.* **1991**, *87*, 3875.
(19) Morales, M. P.; Gonzáles-Carreño, T.; Serna, C. J. *J. Mater. Res.* **1992**, *7*, 2538.
(20) Sugimoto, T.; Maramatsu, A. *J. Colloid Interface Sci.* **1996**, *184*, 626.
(21) Ocaña, M.; Morales, M. P.; Serna, C. J. *J. Colloid Interface Sci.* **1999**, *212*, 317.
(22) Jia, C. J.; Sun, L. D.; Yan, Z. G.; You, L. P.; Luo, F.; Han, X. D.; Pang, Y. C.; Zhang, Z.; Yan, C. H. *Angew. Chem., Int. Ed.* **2005**, *44*, 4328.
(23) Kandori, K.; Yasukawa, A.; Ishikawa, T. *J. Colloid Interface Sci.* **1996**, *180*, 446.
(24) Kandori, K.; Nakamoto, Y.; Yasukawa, A.; Ishikawa, T. *J. Colloid Interface Sci.* **1998**, *202*, 499.
(25) Kandori, K.; Yamamoto, N.; Yasukawa, A.; Ishikawa, T. *Phys. Chem. Chem. Phys.* **2002**, *4*, 6116.
(26) Musić, S.; Krehula, S.; Popović, S.; Skoko, Ž. *Mater. Lett.* **2003**, *57*, 1096.
(27) Wang, X.; Chen, X.; Ma, X.; Zheng, H.; Ji, M.; Zhang, Z. *Chem. Phys. Lett.* **2004**, *384*, 391.
(28) Kandori, K.; Sakai, M.; Inoue, S.; Ishikawa, T. *J. Colloid Interface Sci.* **2006**, *293*, 108.
(29) Pu, Z.; Cao, M.; Yang, J.; Huang, K.; Hu, C. *Nanotechnology* **2006**, *17*, 799.
(30) Nakamura, T.; Kurokawa, H. *J. Mater. Sci.* **1995**, *30*, 4710.
(31) de Faria, D. L. A.; Silva, S. V.; de Oliveira, M. T. *J. Raman Spectrosc.* **1997**, *28*, 873.
(32) Bersani, D.; Lottici, P. P.; Montenero, A. *J. Raman Spectrosc.* **1999**, *30*, 355.
(33) Shim, S.-H.; Duffy, T. S. *Am. Mineral.* **2002**, *87*, 318.
(34) Sapieszko, R. S.; Matijević, E. *J. Colloid Interface Sci.* **1980**, *74*, 405.

JP800683J